Supplementary Information for

Surface-Redox Sodium-Ion Storage in Anatase Titanium Oxide

Qiulong Wei[1,2,*], Xiaoqing Chang[1], Danielle Butts[3], Ryan DeBlock[3], Kun Lan[4,5], Junbin Li[1], Dongliang Chao[4], Dong-Liang Peng[1,2], and Bruce Dunn[3,*]

[1]Department of Materials Science and Engineering, Fujian Key Laboratory of Surface and Interface Engineering for High Performance Materials, Xiamen Key Laboratory of High Performance Metals and Materials, College of Materials, Xiamen University, Xiamen 361005, P. R. China

[2]Innovation Laboratory for Sciences and Technologies of Energy Materials of Fujian Province (IKKEM), Xiamen 361005, P. R. China

[3]Department of Materials Science and Engineering, University of California Los Angeles, Los Angeles, CA, 90095, USA

[4]Laboratory of Advanced Materials, Department of Chemistry, State Key Laboratory of Molecular Engineering of Polymers, iChEM (Collaborative Innovation Center of Chemistry for Energy Materials), Fudan University, Shanghai, 200433, P. R. China

[5]College of Chemistry and Chemical Engineering, Inner Mongolia University, Hohhot 010070, P. R. China.

*Correspondence and requests for materials should be addressed to:
Prof. Qiulong Wei, E-mail: qlwei@xmu.edu.cn
Prof. Bruce Dunn, E-mail: bdunn@ucla.edu

Supplementary Section 1. Materials Characterizations

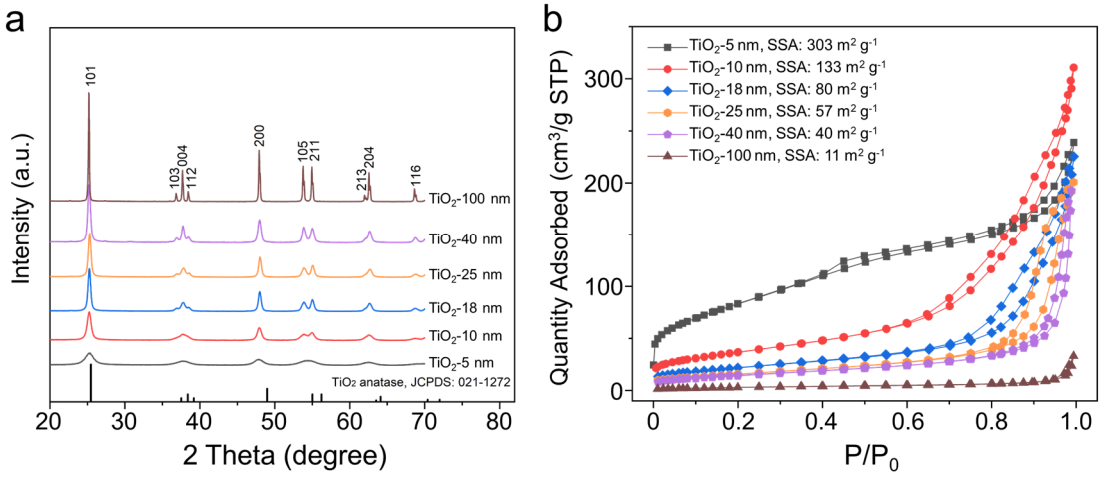

Supplementary Figure 1. (a) XRD patterns of TiO_2 nanoparticles (NPs) and (b) the N_2 adsorption-desorption isotherms of TiO_2 NPs. The average crystallite sizes of the TiO_2 NPs were calculated according to the Scherrer formula $d = 0.9\lambda_{Cu}/\omega$, where d is the crystallite size, λ_{Cu} = 1.5406 Å is the X-ray wavelength, and ω is full width at half-maximum of the diffraction peak. The calculated results of TiO_2 NPs are ~5, 10, 18, 25, 40 and 100 nm, respectively.

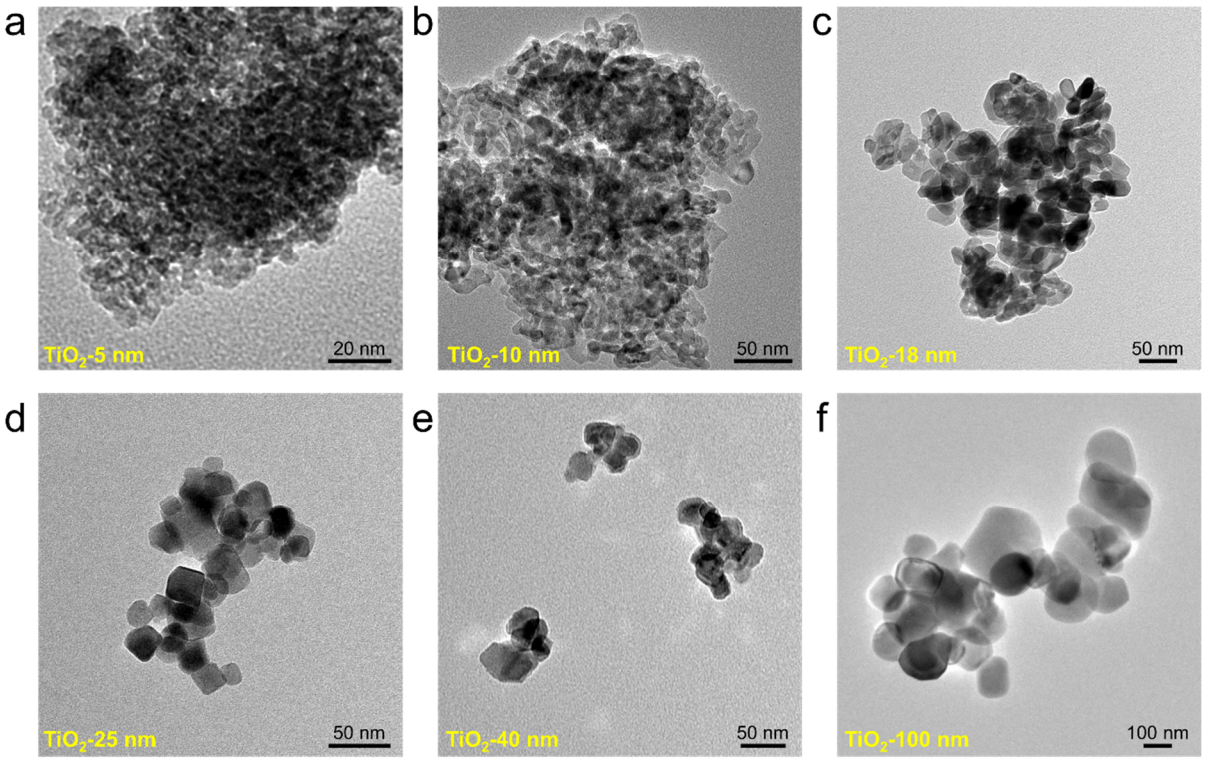

Supplementary Figure 2. TEM images of TiO_2 NPs. (a) TiO_2-5 nm, (b) TiO_2-10 nm, (c) TiO_2-18 nm, (d) TiO_2-25 nm, (e) TiO_2-40 nm, and (f) TiO_2-100 nm.

Supplementary Table 1. Morphology of different TiO_2 NPs.

Sample	NP's size calculated based on Scherrer formula	BET specific surface area (SSA)	NP's size calculated based on SSA
TiO_2-5 nm	4.96 nm	303 m^2 g^{-1}	5.18 nm
TiO_2-10 nm	9.86 nm	133 m^2 g^{-1}	11.81 nm
TiO_2-18 nm	17.93 nm	80 m^2 g^{-1}	19.63 nm
TiO_2-25 nm	24.68 nm	57 m^2 g^{-1}	27.55 nm
TiO_2-40 nm	39.82 nm	40 m^2 g^{-1}	39.27 nm
TiO_2-100 nm	98.23 nm	11 m^2 g^{-1}	142.79 nm

Supplementary Section 2. Electrochemical sodium-ion storage of TiO_2 NPs.

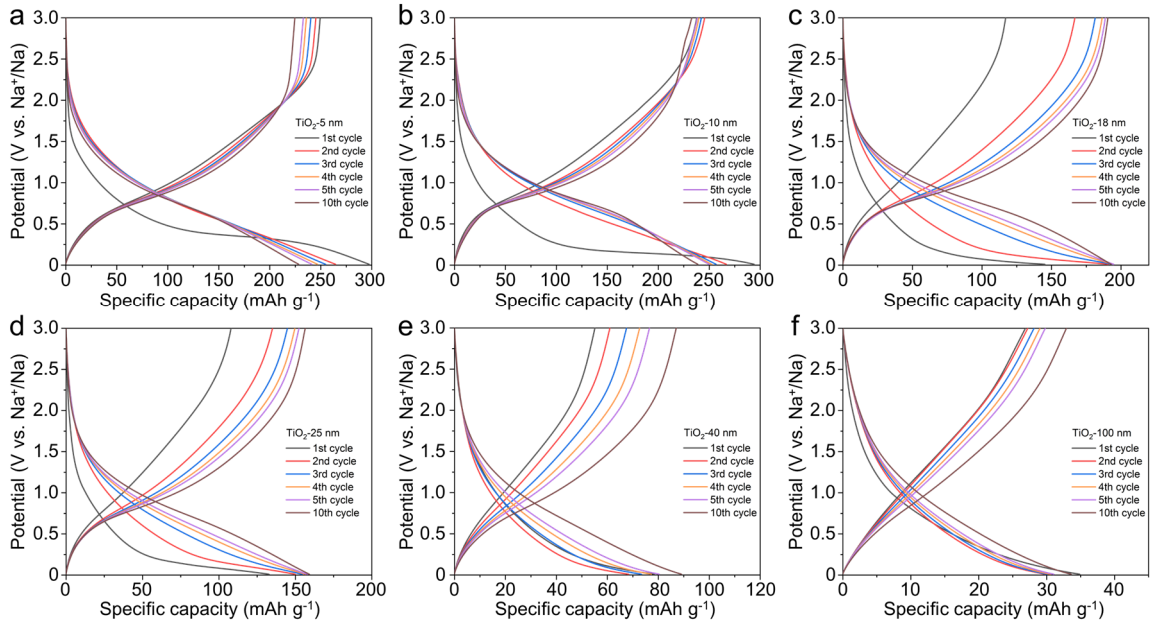

Supplementary Figure 3. Charge and discharge curves of the TiO_2 NPs at 0.1 A g^{-1}: (a) TiO_2-5 nm, (b) TiO_2-10 nm, (c) TiO_2-18 nm, (d) TiO_2-25 nm, (e) TiO_2-40 nm, and (f) TiO_2-100 nm.

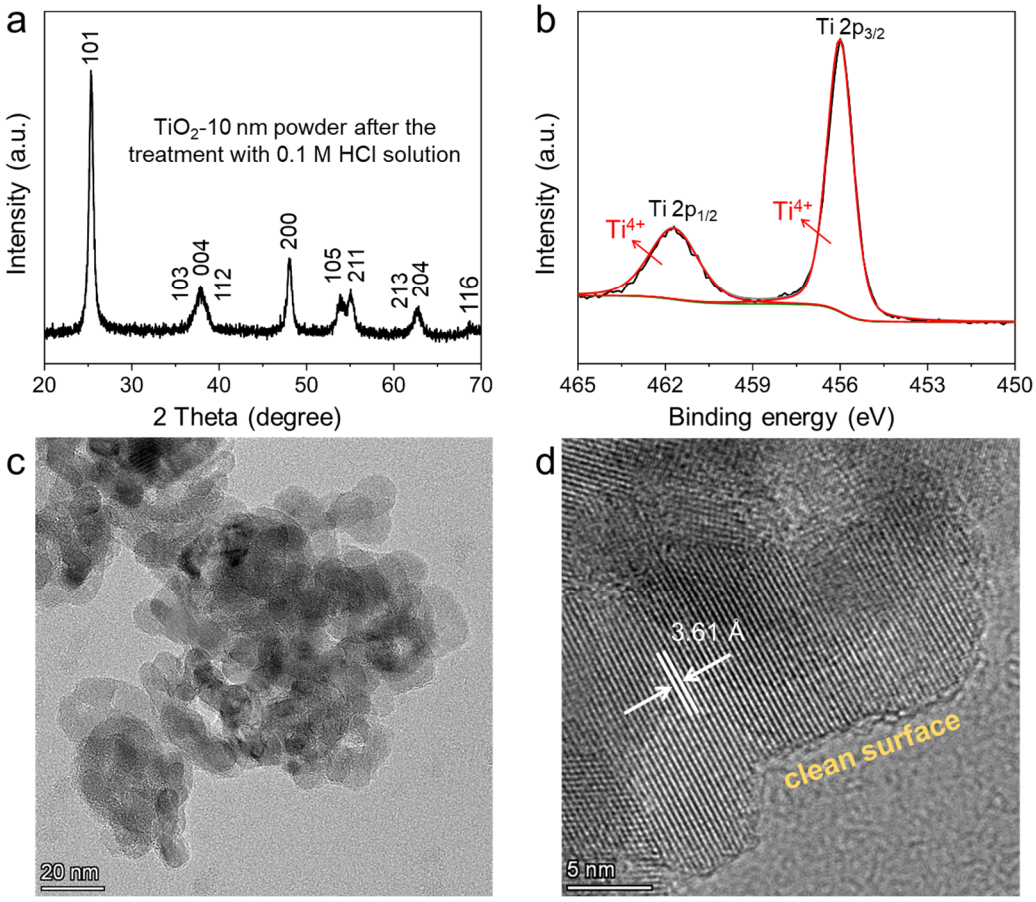

Supplementary Figure 4. XRD pattern (a), Ti 2p spectra (b), TEM image (c) and HRTEM image (d) of TiO_2-10 nm after the treatment with 0.1 M HCl solution. After soaking in 0.1 M HCl solution, the TiO_2-10 nm keeps in anatase phase and its surface remains the valance of Ti^{4+}, indicating the acid treatment has no effects on the TiO_2 NPs.

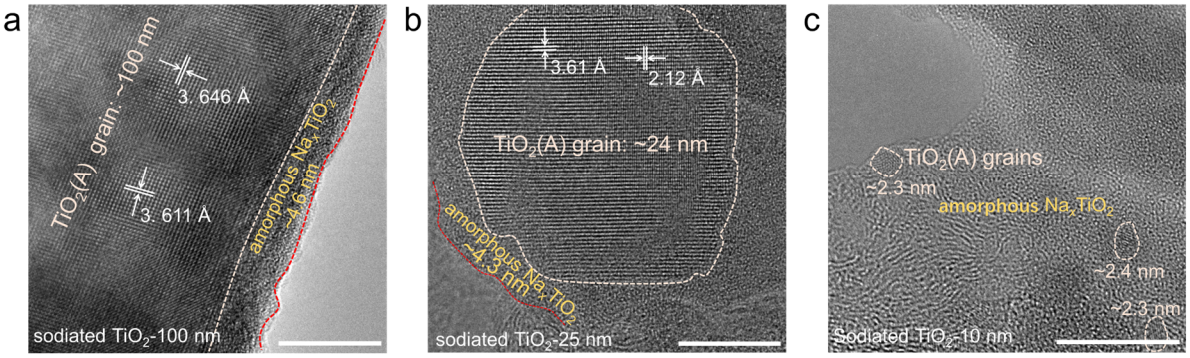

Supplementary Figure 5. The *ex-situ* HRTEM images of TiO_2-100 nm (a), TiO_2-25 nm (b) and TiO_2-10 nm (c) in the fully sodiated state after acid treatment. Scale bar: 10 nm. The amorphous layers are still observed after removing the SEI layers (acid treatment), confirming the amorphous transition is caused by the electrochemically sodiation reaction.

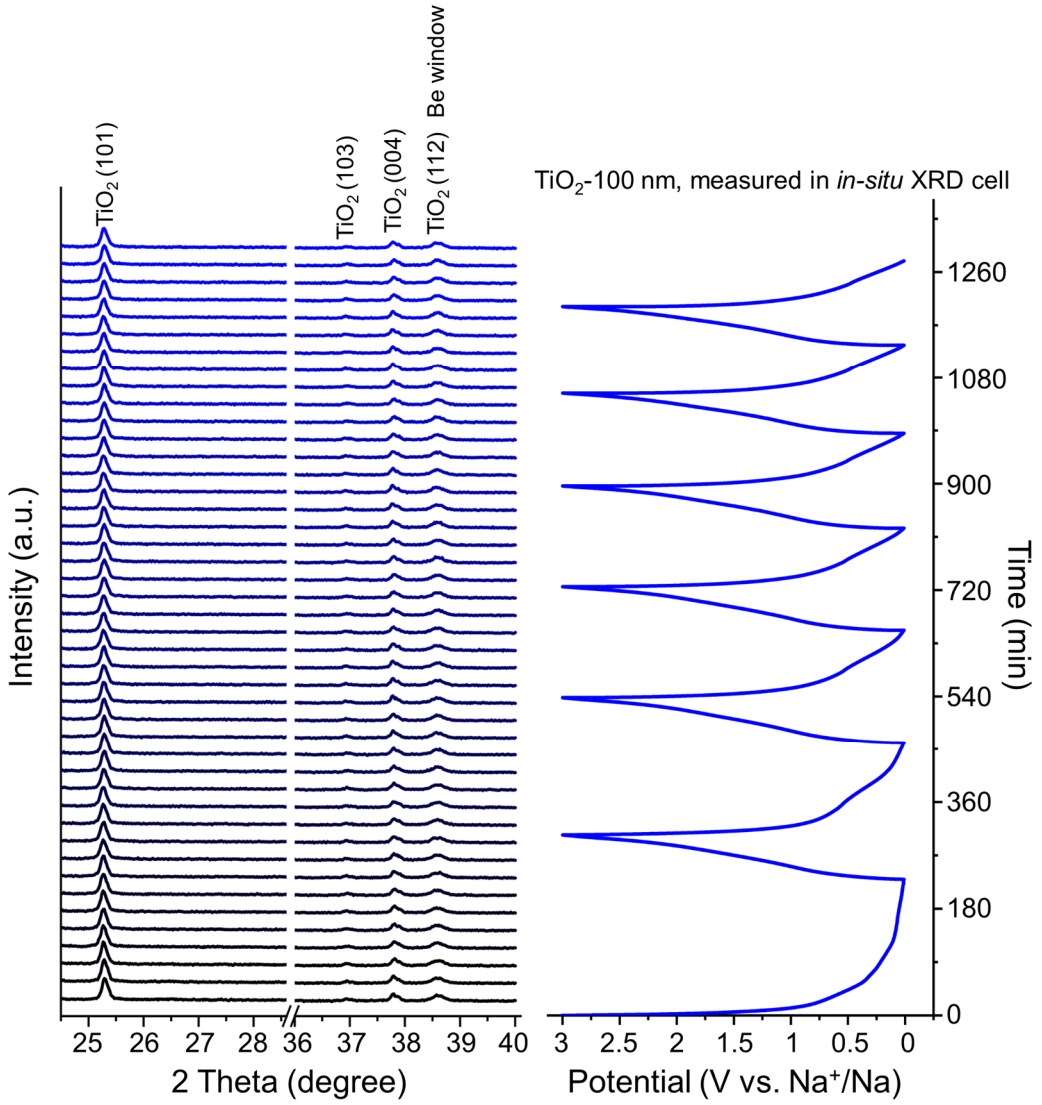

Supplementary Figure 6. *In-situ* XRD patterns of TiO_2-100 nm. The electrochemical performance was measured using an in-situ XRD cell using Be foil as both the X-ray transparent window and current collector. As a result of this cell design, side reactions and electrolyte decomposition were more pronounced, leading to the longer initial sodiation curve when compared to the electrochemical performance measured in coin cell (Supplementary Figure 3f).

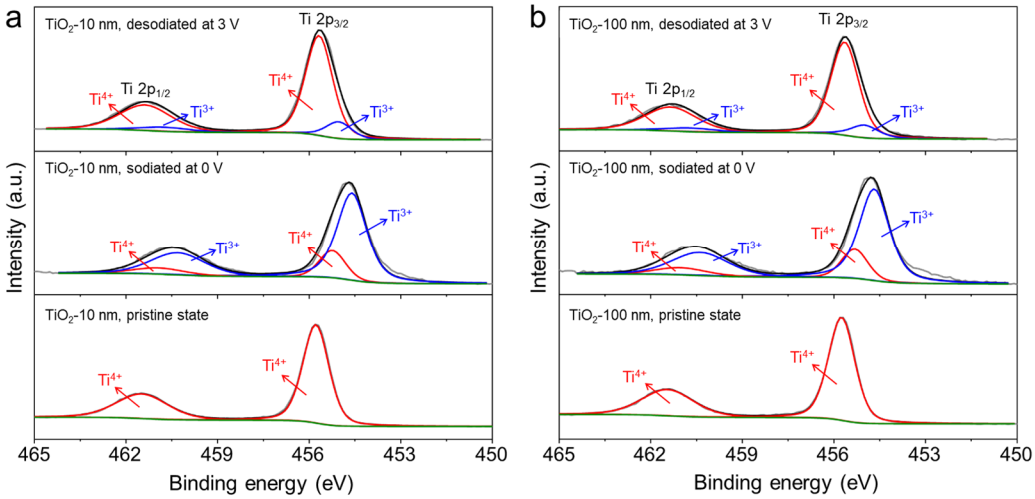

Supplementary Figure 7. Ex-situ XPS spectra analysis. (a) Ti 2p spectra of the TiO_2-10 nm electrode at different states. (b) Ti 2p spectra of the TiO_2-100 nm electrode at different states. Based on the fitting results (Supplementary Table 2), it is found that both materials exhibit the presence of the same amorphous surface composition (Na_xTiO_2 with $x = 0.8$).

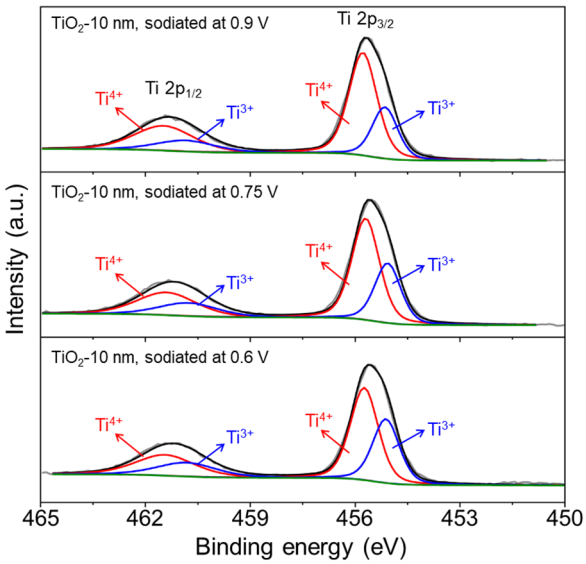

Supplementary Figure 8. Ti 2p spectra of the TiO_2-10 nm electrode at potentials of 0.9 V, 0.75 V and 0.6 V *vs.* Na^+/Na, after 3 cycles. According to Supplementary Table 2, it is found that the sodiation peak at ~0.75 V is mainly based on the redox of Ti^{4+}/Ti^{3+}.

Supplementary Table 2. Analysis of *ex-situ* XPS peaks for the TiO_2-10 nm and TiO_2-100 nm. The peak separation between Ti $2p_{3/2}$ and Ti $2p_{1/2}$ is 5.7 eV and the areas of the peaks are in the ratio of 2:1.

Sample	Position (eV)	Ti $2p_{3/2}$ (4+) 455.8 ± 0.2	Ti $2p_{1/2}$ (4+) 461.5 ± 0.2	Ti $2p_{3/2}$ (3+) 455.1 ± 0.2	Ti $2p_{1/2}$ (3+) 460.8± 0.2
TiO_2 10 nm, pristine state	area	96818	48409	--	--
	percentage	100%		--	
TiO_2 10 nm, sodiated at 0.01 V	area	5466	2733	22904	11452
	percentage	19.3%		80.7%	
TiO_2-10 nm, desodiated at 3 V	area	53980	26990	8590	4295
	percentage	86.3%		13.7%	
TiO_2-100 nm, pristine state	area	55720	27860	--	--
	percentage	100%		--	
TiO_2-100 nm, sodiated at 0.01 V	area	1996	998	8114	4057
	percentage	19.7%		80.3%	
TiO_2-100 nm, desodiated at 3 V	area	17670	8835	2650	1325
	percentage	87.0%		13.0%	
TiO_2-10 nm, sodiated at 0.9 V	area	22256	11128	9835	4917.5
	percentage	69.4%		30.6%	
TiO_2-10 nm, sodiated at 0.75 V	area	20796	10398	11444	5722
	percentage	64.5%		35.5%	
TiO_2-10 nm, sodiated at 0.6 V	area	19322	9661	12940	6470
	percentage	59.9%		40.1%	

Supplementary Table 3. The specific capacity of the TiO_2 NPs (this work) and previously reported TiO_2 with different particle sizes.

Sample	Particle size (nm)	Specific surface area ($m^2\ g^{-1}$)	Specific capacity (mAh g^{-1})	Testing conductions	Electrode composite
TiO_2-5 nm [this work]	4.96*	303	265	at 100 mA g^{-1} in 0.01-3 V	TiO_2:KJB:CMC:SBR =85:7:4:4
TiO_2-10 nm [this work]	10.21*	133	264		
TiO_2-18 nm [this work]	17.93*	80	195		
TiO_2-25 nm [this work]	24.68*	57	161		
TiO_2-40 nm [this work]	39.82*	40	102		
TiO_2-100 nm [this work]	98.23*	11	40		
TiO_2(A) NPs (30 nm) [1]	30	--	150	at 33.5 mA g^{-1} in 0.1-2 V	TiO_2:Super C65:CMC =70:20:10
TiO_2(A)@C NPs (~11 nm) [2]	11	119.8	227	at 33.5 mA g^{-1} in 0.05-2 V	TiO_2:Super C65:PVdF =65:25:10
TiO_2(A) NPs (<25 nm) [3]	<25	--	192	at 0.1 A g^{-1} in 0.01-3 V	TiO_2:CB:PVdF =70:20:10
TiO_2(A) NPs (22.5 nm) [4]	22.5*	80.72	188	at 33.6 mA g^{-1} in 0.01-3 V	TiO_2:SP:CMC =70:15:15
TOC-80 [5]	15*	124	243	at 84 mA g^{-1} in 0.01-2.5 V	TiO_2:SP:CMC =70:15:15
TOC-150 [5]	19*	76	223		
TOC-300 [5]	22*	61	187		

* calculated based on Scherrer formula; CB: carbon black

References

1. Wu, L. *et al.* Unfolding the mechanism of sodium insertion in anatase TiO_2 nanoparticles. *Adv. Energy Mater.* **5**, 1401142 (2015).
2. Tahir, M. N. et al. Extraordinary performance of carbon-coated anatase TiO2 as sodium-ion anode. Adv. Energy Mater. 6, 1501489 (2016).
3. Xu, Z.-L. *et al.* Engineering solid electrolyte interphase for pseudocapacitive anatase TiO_2 anodes in sodium-ion batteries. *Adv. Funct. Mater.* **28**, 1802099 (2018).
4. Chen, J. *et al.* Black Anatase titania with ultrafast sodium-storage performances stimulated by oxygen vacancies. *ACS Appl. Mater. Inter.* **8**, 9142-9151 (2016).
5. Chen, J. *et al.* Size-tunable olive-like anatase TiO_2 coated with carbon as superior anode for sodium-ion batteries. *Small* **12**, 5554-5563 (2016).

Supplementary Section 3. Kinetics analysis for the sodium-ion storage of TiO_2 NPs.

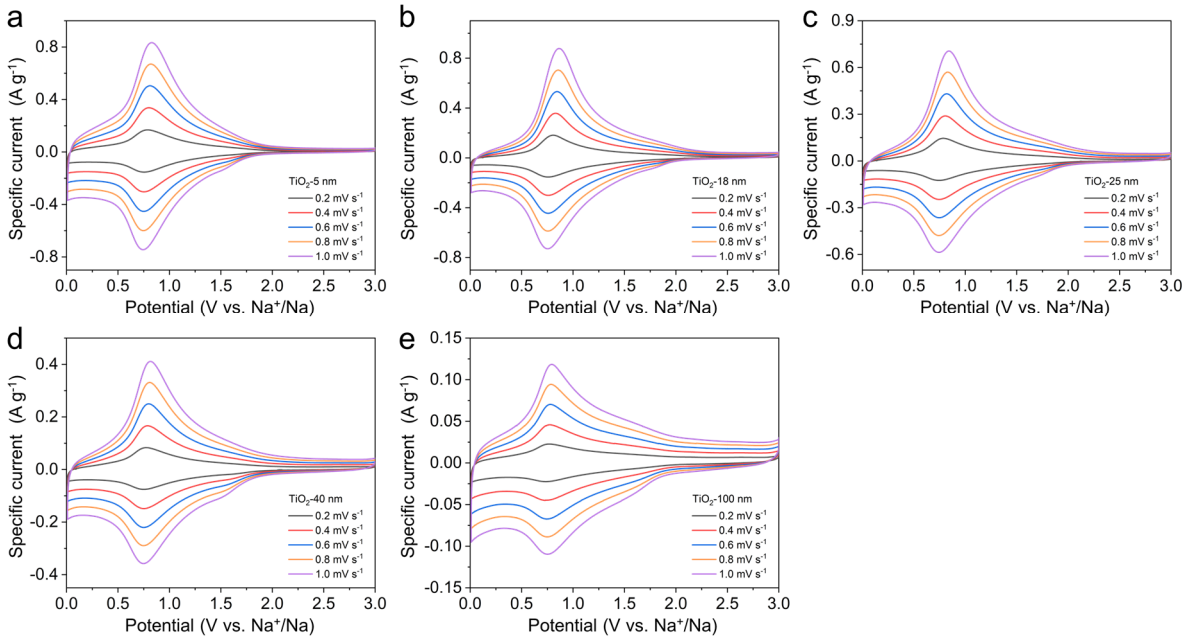

Supplementary Figure 9. CV curves for the sodium-ion storage of TiO_2-NPs at sweep rates from 0.2 to 1 mV s^{-1}: (a) TiO_2-5 nm, (b) TiO_2-18 nm, (c) TiO_2-25 nm, (d) TiO_2-40 nm, and (e) TiO_2-100 nm.

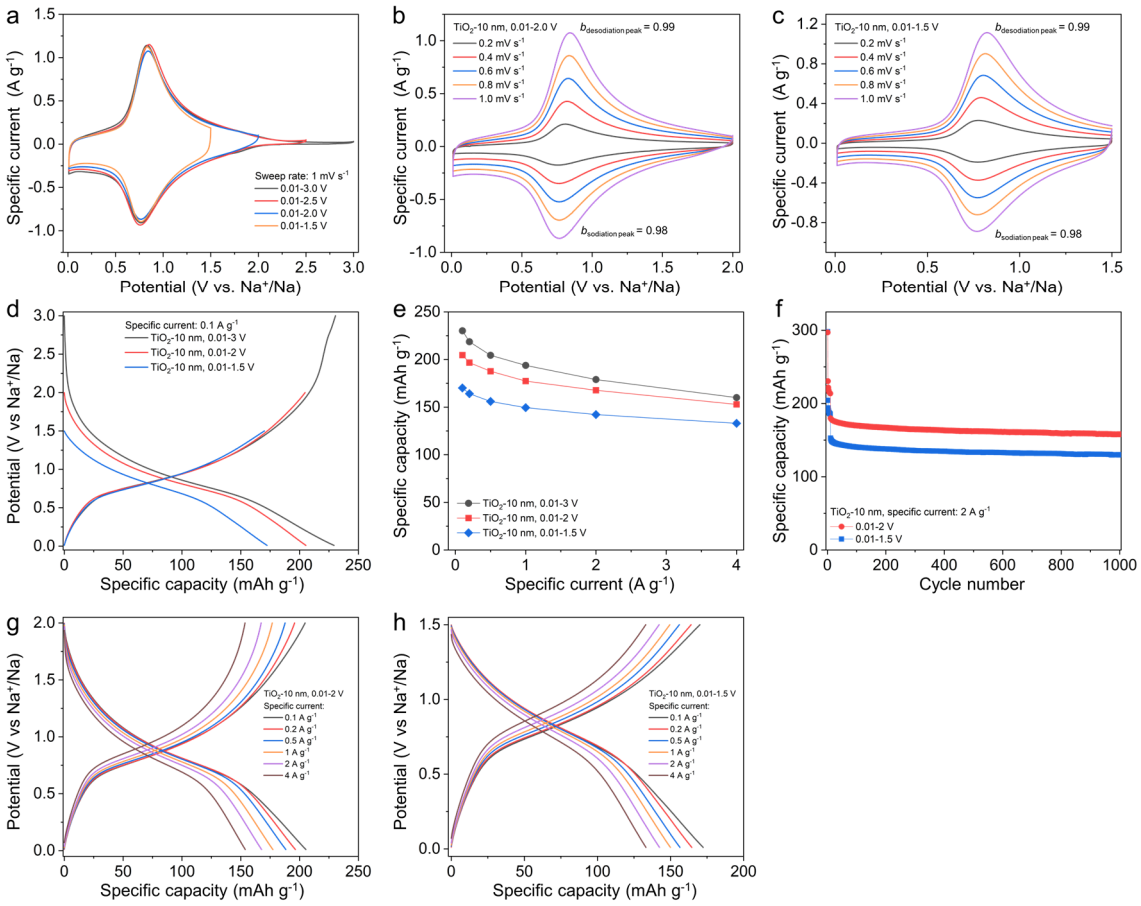

Supplementary Figure 10. (a) CV curves of TiO_2-10 nm in different potential windows, at 1 mV s^{-1}. The CV curves of TiO_2-10 nm in 0.01-2 V (b) and 0.01-1.5 V (c), at sweep rates ranging from 0.2 to 1.0 mV s^{-1}. (d) Charge and discharge curves of TiO_2-10 nm in different potential windows at 0.1 A g^{-1}. The rate capabilities (e) and cycling performance of TiO_2-10 nm at 2 A g^{-1} (f) in different potential windows. Charge and discharge curves of TiO_2-10 nm in 0.01-2 V (g) and 0.01-1.5 V (h), respectively.

The TiO_2-10 nm anodes display the coupled redox peaks in different potential windows, indicating the highly reversible surface-redox reactions. According to the kinetics analysis, the TiO_2-10 nm anodes also exhibit surface-controlled kinetics in the range of 0.01-2.0 V (Supplementary Fig. 10b) and 0.01-1.5 V (Supplementary Fig. 10c). The charging and discharging curves show the reversible redox reaction in the different potential ranges (Supplementary Figure 10d). Meanwhile, the TiO_2-10 nm anodes showed excellent rate capability and cycling stability in the different potential ranges (Supplementary Figure 10e-h).

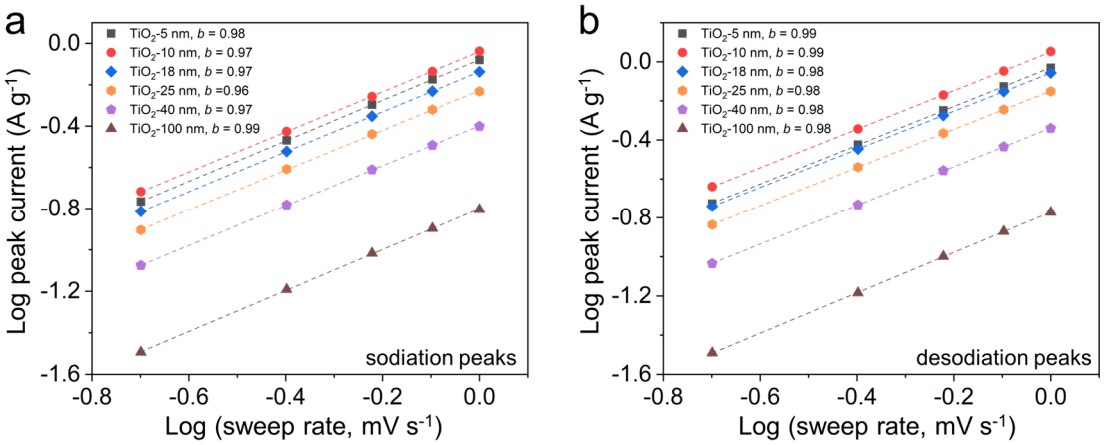

Supplementary Figure 11. *b*-value fitting of the sodiation peaks (a) and desodiation peaks (b) of the TiO_2 NPs, respectively.

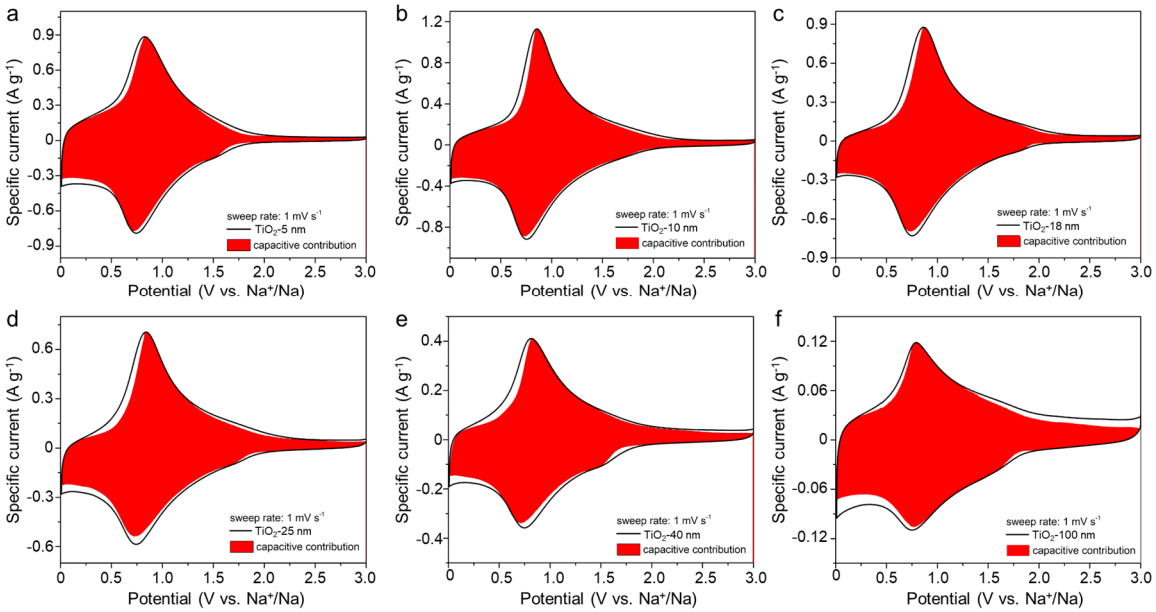

Supplementary Figure 12. Capacitive contributions to sodium-ion storage for TiO_2 NPs at 1.0 mV s^{-1}, (a) TiO_2-5 nm, (b) TiO_2-10 nm, (c) TiO_2-18 nm, (d) TiO_2-25 nm, (e) TiO_2-40 nm, and (f) TiO_2-100 nm.

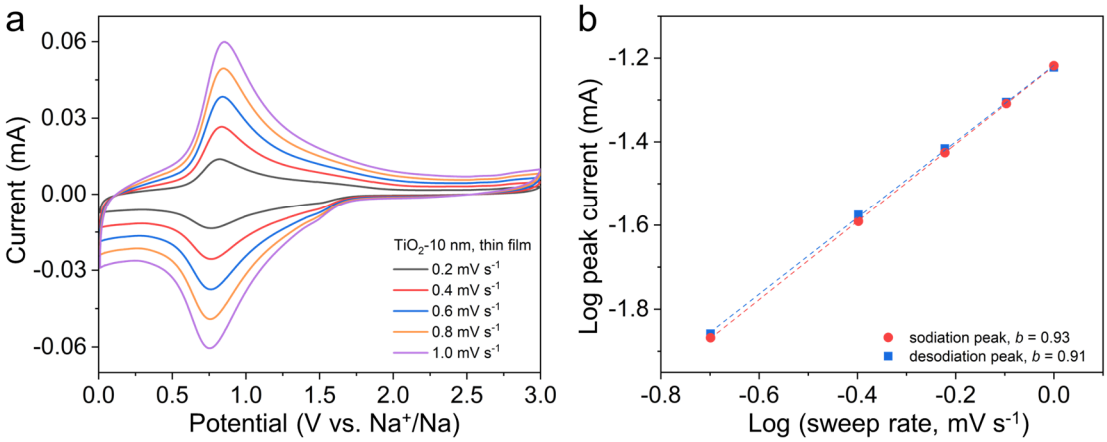

Supplementary Figure 13. (a) CV curves for the thin-film electrode of TiO_2-10 nm (100 μg cm^{-2}, without any binder or carbon additives), at sweep rates from 0.2 to 1 mV s^{-1}. (b) The corresponding *b*-value fitting of the sodiation and desodiation peaks for the thin-film electrode.

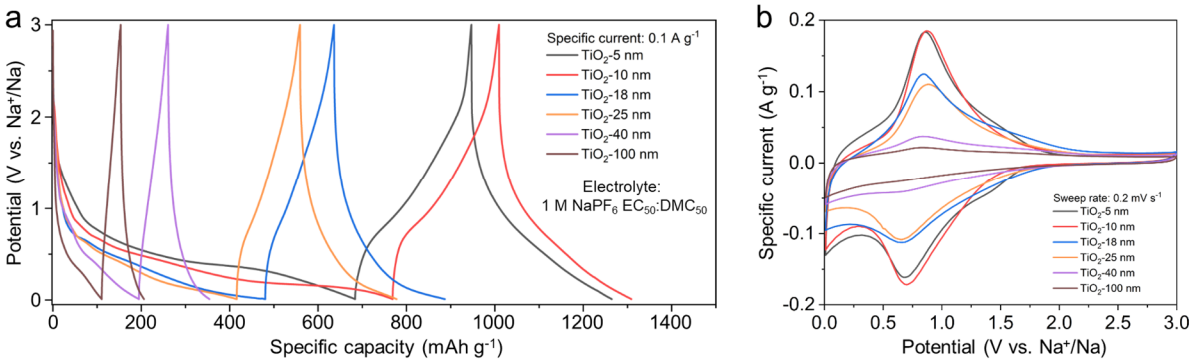

Supplementary Figure 14. The initial sodiation and desodiation curves at 0.1 A g^{-1} (**a**) and CV curves at the sweep rate of 0.2 mV s^{-1} (**b**) of different TiO_2 NPs measured in the electrolyte of 1 M $NaPF_6$ in EC_{50}:DMC_{50}. The initial discharge capacity of TiO_2 NPs in ester-based electrolyte (Supplementary Figure 13a) is higher than those in ether-based electrolyte (Figure 1a), owing to the serious decomposition of carbonate electrolyte and the formation of thick SEI layers. Moreover, the specific capacity of TiO_2 NPs in ester-based electrolyte is size-dependent as well. The CV curves of the TiO_2 NPs measured in ester-based electrolyte (Supplementary Figure 13b) show a similar shape and redox reaction potential compared to those in ether-based electrolyte (Figure 4a). These results indicate that the electrolyte system does not affect the surface-redox sodium-ion storage mechanism of anatase. However, the as-formed thick SEI layers from the ester-based electrolyte (1 M $NaPF_6$ in EC_{50}:DMC_{50}) limit the rate performance.

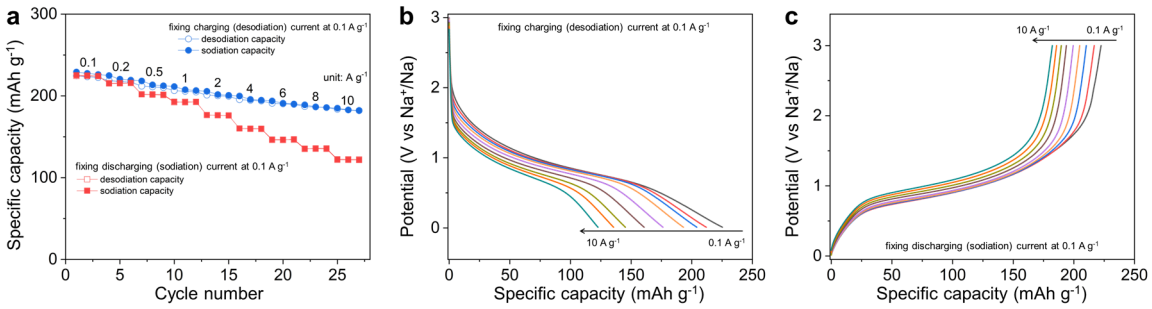

Supplementary Figure 15. (a) Capacity plots with different discharge (sodiation) and charge (desodiation) currents. (b) The discharge curves of TiO_2-10 nm though fixing the charge (desodiation) current at 0.1 A g^{-1}. (c) The charge curves of TiO_2-10 nm though fixing the discharge (desodiation) current at 0.1 A g^{-1}.

When the desodaition current is fixed at 0.1 A g^{-1}, the TiO_2-10 nm anode exhibits fast sodiation performance (Supplementary Figure 15b): a high capacity of 160 mAh g^{-1} at 4 A g^{-1} and 121 mAh g^{-1} at 10 A g^{-1} (corresponding to a time of 44 seconds to reach 54% of total capacity). Furthermore, when the sodiation current is fixed at 0.1 A g^{-1} (close to full storage of Na^+ in TiO_2), the TiO_2-10 nm anode delivers high desodiation capacity at high rates (Supplementary Fig. 15c), *e.g.* a high capacity of 182 mAh g^{-1} at 10 A g^{-1}, showing the excellent high-rate ability. Comparing the two results in Supplementary Figure 15a and b, the stored capacity of TiO_2 is dependent on the sodiation rates.

Supplementary Section 4. Kinetics analysis for the lithium-ion storage of TiO_2 NPs.

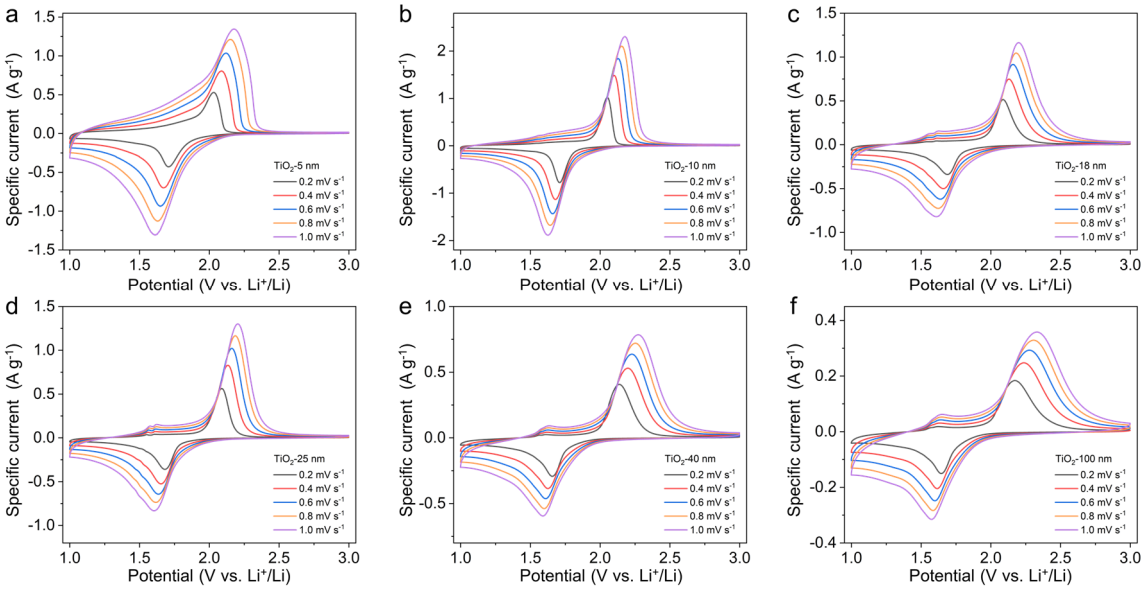

Supplementary Figure 16. The CV curves for the lithium-ion storage of TiO_2 NPs at sweep rates from 0.2 to 1 mV s^{-1}: (a) TiO_2-5 nm, (b) TiO_2-10 nm, (c) TiO_2-18 nm, (d) TiO_2-25 nm, (e) TiO_2-40 nm, and (f) TiO_2-100 nm.

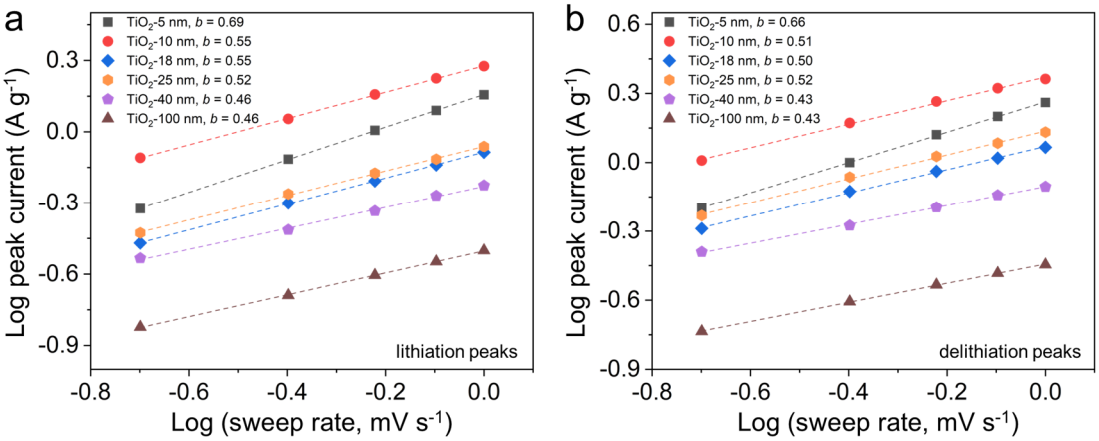

Supplementary Figure 17. The *b*-value fitting of the lithiation peaks (a) and delithiation peaks (b) of the TiO_2 NPs, respectively.

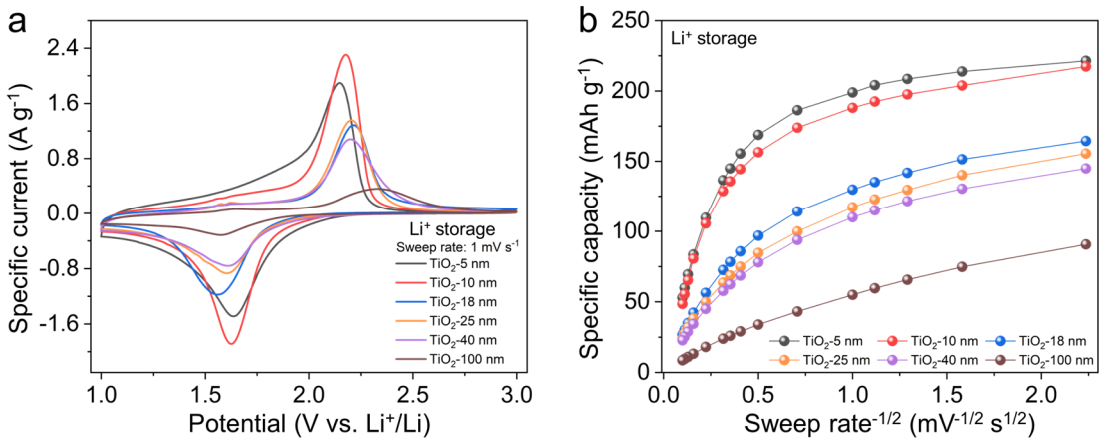

Supplementary Figure 18. (a) The CV curves of the different TiO_2 NPs for lithium-ion storage at a sweep rate of 1 mV s^{-1}. (b) Specific capacity *vs.* sweep rate$^{-1/2}$ curves of the TiO_2 NPs.

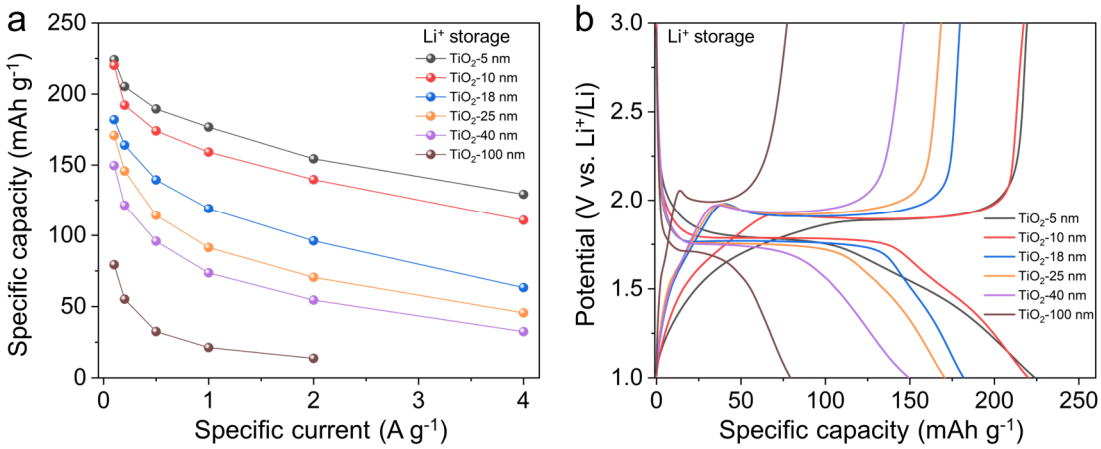

Supplementary Figure 19. (a) The rate capability of the different TiO_2 NPs for lithium-ion storage. (b) The corresponding charge and discharge curves of the TiO_2 NPs at a specific current of 0.1 A g^{-1}.